ARTICLE

OBC
www.rsc.org/obc

Dissociative electron transfer to and from pyrimidine cyclobutane dimers: An electrochemical study

Fabien Boussicault,[a] Oliver Krüger,[b] Marc Robert*[a] and Uta Wille*[c]

[a] *Laboratoire d'Electrochimie Moléculaire, UMR - CNRS No 7591, Université de Paris 7 - Denis Diderot, 2 place Jussieu, 75251 Paris Cedex 05, France. E-mail: robert@paris7.jussieu.fr; Fax: + 33 1 44 27 76 25*

[b] *Institut für Organische Chemie, Universität Kiel, Olshausenstr. 40, 24098 Kiel, Germany*

[c] *School of Chemistry, The University of Melbourne, Victoria 3010, Australia. E-mail: uwille@unimelb.edu.au*

Received 10th May 2004, Accepted 15th July 2004
First published as an Advance Article on the web 31 August 2004

Cyclic voltammetry was used to study the reduction and oxidation behaviour of several pyrimidine cyclobutane dimers mimicking UV induced lesion in DNA strands in polar solvents (*N*,*N*-dimethylformamide and acetonitrile). Both electron injection and removal to and from the dimers, respectively, lead to their cleavage and reformation of the monomeric base. The influence of stereochemistry and substitution pattern at the cyclobutane motif on the reactivity has been studied. It appears that the repair process always proceeds in a sequential fashion with initial formation of a dimer ion radical intermediate, which then undergoes ring opening by homolytic cleavage of the two C–C bonds. Standard redox potentials for the formation of both radical anion and radical cation state of the dimers were determined. Quantum calculations on simplified model compounds reveal the reason for the finding that the exergonic homolytic cleavages of the carbon–carbon bonds are endowed with sizeable activation barriers. The consequences of these mechanistic studies on the natural enzymatic repair by photolyase enzyme are discussed.

Introduction

Major DNA lesions caused by UV (A or B) irradiation are bipyrimidine products (Scheme 1). Among them, the *cis–syn* thymine–thymine cyclobutane dimer, resulting from 2π + 2π cycloaddition of two adjacent bases in the same oligonucleotide strand, appears as the main photoproduct.[1,2] In addition to the classical excision repair mechanism, redox photolyase enzymes are also able to repair these damages in bacteria in a catalytic electron transfer cycle. Inside the enzymatic pocket, fully reduced flavine cofactor ($FADH^-$) is excited by a photon to its singlet state, which transfers one electron to the dimer, T<>T (Scheme 2). Splitting ensues, and the two DNA bases are finally restored after reoxidation of the radical anion of the monomer, $T^{\bullet -}$.[2] This general picture is also supposed to be valid for the repair of 6–4 photoproducts, which are believed to be converted to oxetane or azetidine cyclic structures, prior to their photoreduction by $^1FADH^-*$.[2c,3]

Beside the questions of the ability of the enzyme to recognize and bind to modifed DNA sequences and the exact configuration

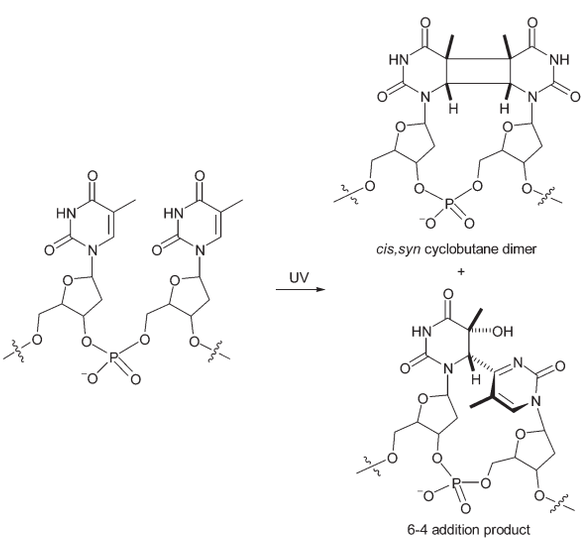

Scheme 1 Main photoproducts obtained from UV induced dimerization of pyrimidine bases in the DNA.

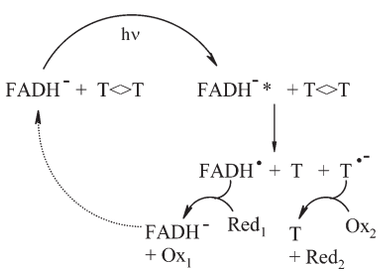

Scheme 2 Catalytic cycle for photoreparation of a thymine dimer (T<>T) by a flavin cofactor ($FADH^-$) in a photolyase enzyme.

of the cofactor inside the enzyme pocket relative to the lesion, the microscopic aspects of the reaction are still not fully understood. In particular, is the charge transfer and the breaking of the dimer (which implies two homolytic C–C bond cleavages) concerted or not (Scheme 3)?[4] If not, how does the stereochemistry of the dimer (*cis vs. trans*, *syn vs. anti*, see below) affect the cleavage rate? And what are the reasons why these homolytic breakages may possess sizable activation barriers? Whereas photolyase type enzymes are able to reductively repair DNA photoproducts, it has also been shown that pyrimidine cyclobutane dimer splitting could be induced by oxidation.[5a] For example, the nitrate radical $NO_3^{\bullet}$ is a powerful oxidant able to irreversibly cleave *N*,*N*-dimethyl-substituted uracil cyclobutane dimers, DMU<>DMU.[5b] The same questions arise concerning the possible simultaneousness of the electron removal from the dimer and the cleavage of the cyclobutane ring, as well as on the role of the stereochemistry at the ring. It should be noted that such charge induced cleavage of cyclobutane containing small organic molecules have already been reported, both under reductive[5c] and oxidative conditions.[5d–f]

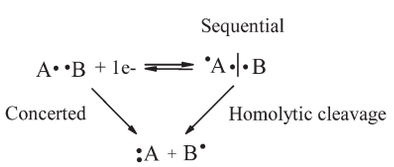

Scheme 3 Reductive cleavage of a molecule AB (the electron donor could be either an electrode, the excited state of an aromatic molecule or an homogeneous donor).

DOI: 10.1039/b406923d

Beyond these mechanistic questions, bipyrimidine dimers are interesting structures for studying excess electron transfer in DNA, *i.e.* the hopping of a negative charge through the bases over long distances.[6] Carell *et al.* pioneered this emerging field by studying charge transfer in DNA hairpins containing a *cis–syn* thymine dimer and a flavin, covalently attached to the head of the hairpin at a controlled distance from the lesion.[7] The redox reaction is triggered from UV irradiation and its efficiency could be quantified through measurement of cleaved DNA strands as a function of time.

In an effort to better understand the mechanism of the chemical repair of bipyrimidine lesions, we have performed direct electrochemistry (cyclic voltammetry) on model lesion compounds possessing different substitution pattern and stereochemistry at the cyclobutane ring (*e.g. N*,*N*-dimethylated uracil, 6-methyl uracil and thymine cyclobutane dimers, see Scheme 4) as well as on selected pyrimidine monomers (*e.g. N*,*N*-dimethylated and non methylated uracil and thymine) at glassy carbon electrodes. The mechanisms have been studied in *N*,*N*-dimethylformamide (DMF) in the case of the reductive processes and in acetonitrile (ACN) in the case of the oxidative repair.

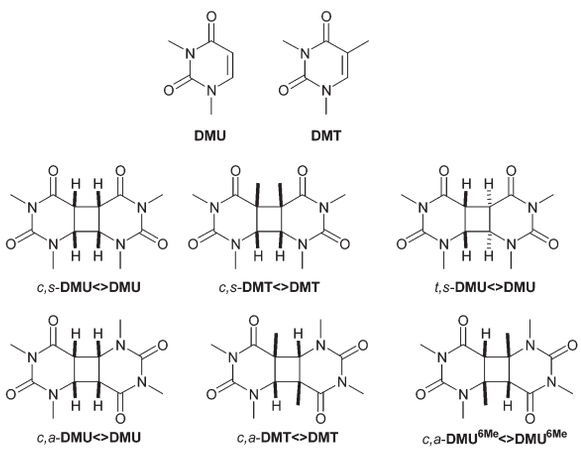

Scheme 4 *N*,*N*′-methylated pyrimidine monomers and dimers investigated.

In a first part, we'll briefly describe the reduction and oxidation mechanism of the monobases. Elving *et al.* carefully studied the electrochemistry of DNA bases in polar aprotic solvent.[8a,b] We get back to these studies by looking at the effect of methyl substitution onto the two nitrogen atoms. From there, we'll turn to the electrochemical activity of the model dimers. We'll take advantage of a careful analysis of the voltammograms and of their characteristics as a function of the scan rate in order to decipher the exact mechanism by which these compounds are reduced and oxidized. In addition, density functional theoretical calculations (B3LYP) for simplified model compounds were performed to theoretically describe the potential energy surfaces involved. These calculations will prove to be useful for underlying the reasons why such exergonic homolytic cleavages may be endowed with non zero activation barriers.

Experimental results

All substrates were studied by cyclic voltammetry at 3 mm diameter glassy carbon electrodes in *N*,*N*′-dimethyl formamide (DMF, reduction) or acetonitrile (ACN, oxidation). For details, see Experimental section.

Electron transfer to and from DNA thymine and uracil bases and *N*,*N*′-methylated bases at carbon electrodes

N,*N*-dimethyl uracil (DMU) is reduced at very negative potentials, in an irreversible process. As shown in Fig. 1, the wave is thin (the peak-width, $E_{p/2}$–E_p, is close to 55 mV at low scan rates). The peak potential (−2.32 V *vs.* SCE at 0.1 V s^{-1}) moves toward negative values at the rate of 31 mV per decade log *v* between 50 mV s^{-1} and 3 V s^{-1}. This behaviour is typical of an *E* + *C* mechanism, where the charge transfer, *E*, is followed by a fast chemical reaction, *C*. The observation that the position of E_p is slightly sensitive to the substrate concentration ($\partial E_p/\partial \log C$ = +8 mV at low scan rates) is an indication for a second order reaction.

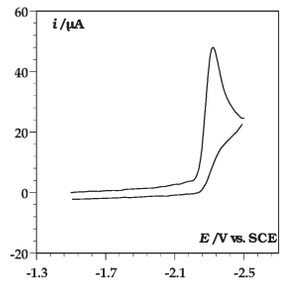

Fig. 1 Cyclic voltammetry of DMU (1.76 mM) in DMF + 0.1 M n-Bu_4NBF_4. Scan rate: 0.1 V s^{-1}. Temperature: 22 °C.

Electron stoichiometry could be obtained from comparison with the fully reversible one electron wave of benzoquinone, for which the peak current is given by[9]

$$i_p = 0.446\, FSC^0 D^{1/2}(Fv/RT)^{1/2} \quad (1)$$

(i_p: peak current, *S*: electrode surface area, C^0: bulk concentration, *D*: diffusion coefficient, *v*: scan rate). For DMU, the current equals

$$i_p = n\Psi_p FSC^0 D^{1/2}(Fv/RT)^{1/2} \quad (2)$$

The non-dimensional peak current Ψ_p varies from 0.527 to 0.351 as the kinetic control progressively passes from the chemical reaction (pure kinetic conditions) to the charge transfer and was estimated at each scan rate from the peak-width and $\partial E_p/\partial \log v$ values. From this, a value of $n \approx 1$ was obtained, corresponding to a monoelectronic reduction wave. It is likely that the radical anion produced after one electron consumption, $DMU^{\bullet -}$, dimerizes at the C(6) position, since B3LYP calculations performed for the uracil radical anion, $U^{\bullet -}$, in the gas phase revealed that the spin density is mainly localized on this position. (Fig. 2).[10] Moreover, semi-empirical calculations have shown that dimerization at C(6) gives a more stable (less constrained) structure than a coupling involving the two C(4) atoms (Fig. 2). This behaviour is in sharp contrast with that of the non methylated uracil. With this latter compound, we experimentally found that the radical anion formed by injection of one electron protonates from the neutral substrate, taking advantage of the acidic proton at the nitrogen atom N(1).[8] The resulting neutral radical then dimerizes. The stoichiometry of the wave concomitantly drops to half an electron per substrate molecule. Addition of a strong acid to a solution of uracil leads to the increase of the wave height by a factor two as predicted by such a mechanism. It's noteworthy that Elving *et al.* proposed a similar mechanism for uracil reduction in dimethylsulfoxide.[8a]

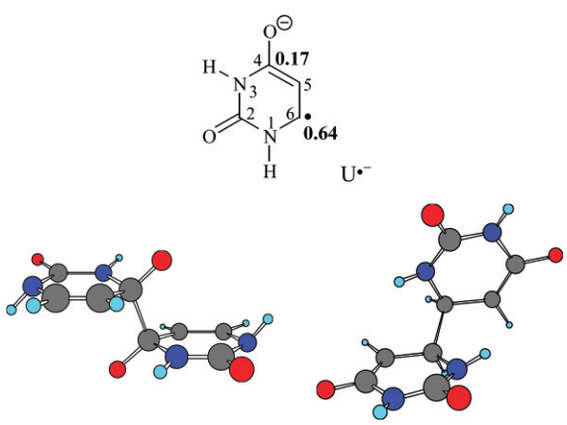

Fig. 2 Top, spin density (bold numbers) on C(4) and C(6) atoms for uracil radical anion, $U^{\bullet -}$ (B3LYP/6–31G*, gas phase). Bottom, dimers obtained from C–C coupling (left: C(4)–C(4)′ coupling; right: C(6)–C(6)′ coupling, favoured).

The reduction behaviour of *N*,*N*-dimethyl thymine (DMT) is very similar to that of DMU, with a very negative reduction wave at about −2.41 V *vs* SCE (0.1 V s^{-1}). The peak-width was 52 mV at the same scan rate and an E_p variation with scan rate and substrate concentration of about −26 mV and 12 mV per decade log, respectively. The number of electrons exchanged per reduced starting molecule is $n = 1.05$, suggesting a similar mechanism as with DMU. Since the dimerization step may change only marginally (due to the presence of a methyl group adjacent to the C(4) atom) and since the rate of electron transfer should be very close to that of DMU, it may be concluded that the reduction is intrinsically more difficult, which is reflected by the one hundred mV difference in peak potential values between DMU and DMT. A typical voltammetric response is shown on Fig. 3 (upper left curve).

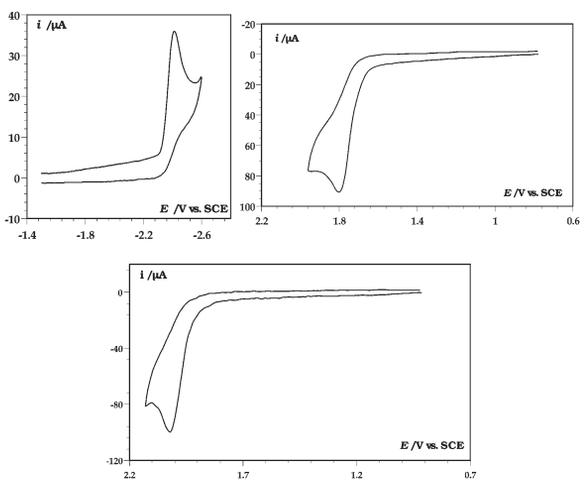

Fig. 3 Top: Cyclic voltammetry of DMT (1.67 mM) in DMF + 0.1 M n-Bu_4NBF_4 (left); DMT (1.96 mM) in ACN + 0.1 M n-Bu_4NBF_4 (right). Bottom: Cyclic voltammetry of DMU (2.06 mM) in ACN + 0.1 M n-Bu_4NBF_4. Scan rate: 0.1 V s^{-1}. Temperature: 22 °C.

Upon oxidation, both DMU and DMT show anodic waves. Oxidation of DMU is difficult, as is reflected by the very positive peak potentials (Fig. 3, $E_p = 2.01$ V *vs.* SCE at 0.1 V s^{-1}). The peak-width, $E_p - E_{p/2}$, is close to 55 mV at low scan rates, and the peak potential shifts to more positive values with 24 mV per decade log *v*. This is the signature of a mixed kinetic control between the first charge transfer and a following chemical reaction. Since E_p does not change with varying substrate concentrations, the chemical reaction should be a first order or pseudo first order reaction. Comparison of the wave height with the reversible one electron reduction of benzoquinone in the same solvent leads to the conclusion that the oxidation of DMU is a bielectronic process with $n = 2.1$. A likely mechanism involves the removal of an electron, followed by rapid loss of a proton from the methyl group linked to the nitrogen N(1) atom and a second oxidation (Scheme 5).[5] The product (DMU^+) may slowly hydrolyze, a reaction not observed on the time scale of cyclic voltammetry.

The C(5) methylated base, DMT, follows a similar mechanism upon oxidation (Fig. 3). The potential is markedly less positive,

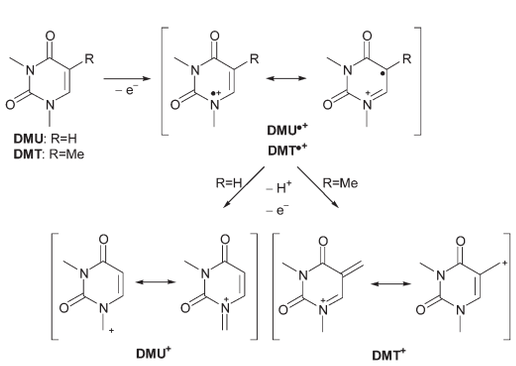

Scheme 5 Oxidation mechanisms of DMU and DMT.

compared to DMU, with 1.81 V *vs.* SCE at 0.1 V s^{-1}. The wave is thin (E_p–$E_{p/2}$ is close to 65 mV at 0.1 V s^{-1}) and drives smoothly to positive potentials with increasing scan rates ($\partial E_p/\partial \log v \approx 25$ mV). The process involves the abstraction of two electrons per substrate molecule ($n = 2.07$).

The 200 mV difference in peak potential values between DMT and DMU certainly reflects the fact that the spin density of the radical cation formed after the loss of the first electron is mainly concentrated on the C(5) atom (about 60% of the total density), as was confirmed by quantum calculations. Thus, in $DMT^{\bullet+}$ the radical is tertiary and secondary in $DMU^{\bullet+}$, leading to a thermodynamic advantage for the formation of the former over the latter. The oxidation mechanisms for both DMU and DMT are summarized in Scheme 5. After formation of $DMT^{\bullet+}$ and $DMU^{\bullet+}$, respectively, deprotonation is likely to occur; in the case of $DMT^{\bullet+}$ at the C(5)-methyl side chain and in the case of $DMU^{\bullet+}$ presumably at the methyl group at N(1), which is then followed by a second oxidation step.

Dissociative electron transfer to and from cyclobutane pyrimidine dimers at carbon electrodes

The next step consists of a detailed study of the cleavage pathways for various DNA photolesion model compounds (Scheme 4). The methodology and experimental conditions were the same as for the preceeding bases.

***c,s*-DMU◇DMU.** This compound represents a typical example for the behaviour of pyrimidine cyclobutane dimer upon electron injection or removal. It gives rise to two irreversible oxidation waves, located at 1.68 V *vs.* SCE and at 2.02 V *vs.* SCE (scan rate of 0.1 V s^{-1}), respectively, as is illustrated in Fig. 4. The second wave is identical to that observed during DMU oxidation, which indicates that the first wave leads to the clevage of the dimer and formation of DMU. The first peak shifts 52 mV to more positive values per decade log *v*, while the peak-width amounts to 80 mV at low scan rates. Thus, during this first oxidation process, the charge transfer from the substrate to the electrode surface is the rate limiting step (at least when the scan rate is increased to a few hundred mV s^{-1}) and is coupled to a fast and irreversible subsequent chemical reaction. Since E_p is insensitive to the substrate concentration, this reaction is first order. Application of the methodology mentioned above[11] revealed that the first wave is bielectronic ($n = 2.25$).

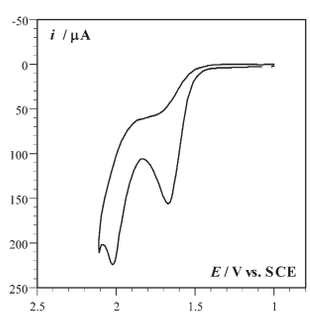

Fig. 4 Cyclic voltammetry of *c,s*-DMU◇DMU (3.46 mM) in ACN + 0.1 M n-Bu_4NBF_4. Scan rate: 0.1 V s^{-1}. Temperature: 22 °C.

On the basis of these observations, a mechanism for *c,s*-DMU◇DMU oxidation is proposed in Scheme 6. The first electron removal leads to the formation of a cation radical, *c,s*-$DMU◇DMU^{\bullet+}$. Then, the C(6)–C(6′) bond next to the oxidized nitrogen atom homolytically breaks, a step endowed with a sizable activation barrier, immediately followed by the homolytic scission of the C(5)–C(5′) bond, which is endowed with a small, if any, activation barrier (see the Discussion section for a justification of the order of bond cleavage). The radical cation $DMU^{\bullet+}$ loses one proton and is subsequently oxidized to an iminium cation DMU^+, which slowly hydrolyses to the mono-methylated uracil MU, as already described for the monobase. The neutral DMU monomer produced by the scission of *c,s*-DMU^+–$DMU^{\bullet}$ is in turn oxidized along the second oxidation wave. Characteristics of this oxidative process

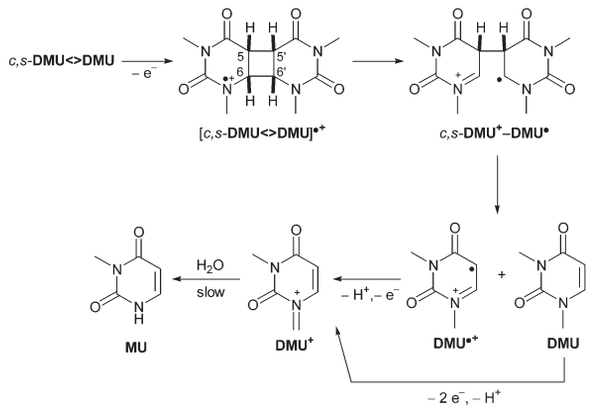

Scheme 6 Oxidation mechanism of *c,s*-DMU◇DMU under electrochemical conditions.

unambiguously show that cleavage of the dimer is a sequential process, charge removing and cleavage step are not concerted.

It was not possible to "trap" the radical cation (*c,s*-DMU◇DMU$^{\bullet+}$) resulting from the first charge transfer because of the quickness of the bond-breaking steps and the slow electron transfer rate. Nevertheless, since the location of the peak is kinetically controlled by the charge transfer above 0.5 V s^{-1}, the following equation may be applied, which relates the peak potential value to the electron transfer rate[9]

$$E_p = E^0_{\text{dimer}^{\bullet+}/\text{dimer}} + 0.78\frac{RT}{\alpha F} - \frac{RT}{\alpha F}\ln\left\{k_s^{\text{app}}\left(\frac{RT}{\alpha F v D}\right)^{1/2}\right\} \quad (3)$$

$E^0_{\text{dimer}^{\bullet+}/\text{dimer}}$ is the standard potential for dimer oxidation, α is the transfer coefficient which is close to 0.5 and k_s^{app} is the standard heterogeneous rate constant for electron flowing. k_s^{app} may vary between 0.15 and 0.30 cm/s (by comparison with molecules of similar size bearing the same functional groups), and the diffusion coefficient D could be evaluated through application of the Stokes–Einstein equation.[11] This leads to a standard potential for the oxidation of *c,s*-DMU◇DMU of

$$E^0_{\text{dimer}^{\bullet+}/\text{dimer}} = 1.82_5 \pm 0.02_5 \text{ V } \textit{vs.} \text{ SCE}$$

It is worth noting that *c,s*-DMU◇DMU is substantially more easily oxidizable than DMU on thermodynamic grounds. Indeed the oxidation peak of DMU is on one hand 200 mV more positive than the standard potential estimated for *c,s*-DMU◇DMU, and on the other hand is less positive than the standard potential of DMU, meaning that there's an important stabilization of the radical cation state in *c,s*-DMU◇DMU$^{\bullet+}$ by the neighbouring base.

Electron injection into *c,s*-DMU◇DMU leads to a reductive wave at very negative potentials (peak potential equals −2.34 V *vs.* SCE at 0.1 V s^{-1}, see Fig. 5). The wave is thin with a peak-width being close to 45 mV at low scan rates and $\partial E_p/\partial \log v \approx -42$ mV. All these observations indicate an E + C mechanism, in which a first electron transfer is followed by a fast chemical reaction and a mixed kinetic control between the E and the C step. Surprisingly, the peak potential is moderately sensitive to the dimer concentration, indicating the interference of a second order reaction. That the reduction process does lead to dimer cleavage and formation of DMU could not be directly confirmed as in the case of oxidation, since DMU is reduced at the same potential than the dimer. However, an electrolysis performed at controlled potential (−2.3 V *vs.* SCE), followed by an oxidative scan revealed the disappearance of the first oxidation wave, which can be explained by a reductive cleavage of the dimer to form DMU. Additionally, the electron stoichiometry, determined from the peak-width and peak shifting with scan rate, indicates a two electron wave (n = 1.85), one electron being used to cleave the dimer, and one electron to reduce the monomer formed. The reductive cleavage is thus two steps, electron transfer and bond breaking are not concerted.

At this point and based on the preceeding analysis, the following mechanism could be proposed (Scheme 7). The first electron

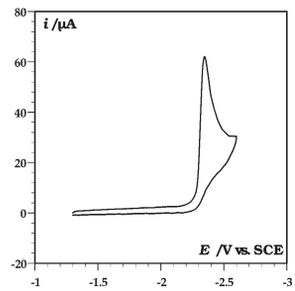

Fig. 5 Cyclic voltammetry of *c,s*-DMU◇DMU (1.70 mM) in DMF + 0.1 M n-Bu_4NBF_4. Scan rate: 0.1 V s^{-1}. Temperature: 22 °C.

is taken up by the carbonyl group at C(4) (π* like orbital),[12] before being transferred into the $\sigma^*_{C(5)-C(5)'}$ orbital. This intramolecular charge transfer is at the origin of the activation barrier.[4c] The C(6)–C(6′) bond then homolytically breaks, concertedly or not with the first cleavage step, to produce both DMU$^{\bullet-}$ and DMU. The first may dimerize to yield a C6–C6-dimer, as previously shown, whereas DMU takes up the second electron before dimerizing likewise. If the two successive C–C cleavages are fast enough, the kinetics of the reaction may well be jointly controlled by the first charge transfer and dimerization of DMU$^{\bullet-}$. This seems to be the case here, as indicated by the slight sensitivity of the peak potential to dimer concentration.

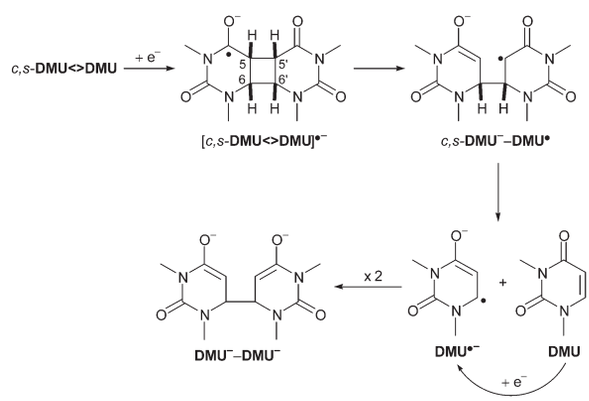

Scheme 7 Reduction mechanism of *c,s*-DMU◇DMU under electrochemical conditions.

Other pyrimidine cyclobutane dimers. *c,a*-DMU^{6Me}◇DMU^{6Me} provides an illustrative example of the modification of both reductive and oxidative voltammetric waves, when the configuration at the cyclobutane motif changes from *syn* to *anti*. Oxidation of *c,a*-DMU^{6Me}◇DMU^{6Me} gives rise to only one irreversible wave, located at 2.02 V *vs* SCE (scan rate 0.1 V s^{-1}), as illustrated in Fig. 6. The peak shifts 45 mV positively per decade log v while the peak-width amounts to 65 mV at low scan rates. Charge transfer from the substrate to the electrode surface is coupled to a fast and irreversible subsequent chemical reaction in a two-step sequence ($E + C$), which jointly control the kinetics of the reaction. Since E_p is insensitive to the substrate concentration, this reaction is of first order. Calculation of the electron stoichiometry revealed release of four electrons per substrate molecule (n = 3.75). This outcome is in contrast to the results of the cleavage of the *c,s*- and *t,s*-configurated dimers, where only two electrons per substrate molecule are exchanged. The reason for this difference is the higher potential required to oxidize *c,a*-DMU^{6Me}◇DMU^{6Me}. One electron is consumed during the actual cleavage of the dimer to form back a neutral monomeric base and a monomeric radical cation, whereas the three others are used to oxidize these products, since they are formed at a potential where they are oxidizable. It is remarkable that *c,a*-DMU^{6Me}◇DMU^{6Me} is oxidized at a potential 340 mV more positive than *c,s*-DMU◇DMU. Not only is the oxidation more difficult on thermodynamic grounds, but it can also be concluded that the splitting of the C(6)–C(6′) bond is slower. Indeed, while intrinsic heterogeneous electron transfer rates are likely to be very close for both *c,s*-DMU◇DMU and

Table 1 Voltammetric data for reduction and oxidation of various *N*,*N*-dimethyl thymine and uracil cyclobutane dimers (at 295 K)

	Reduction [a]				Oxidation [b]			
Compound	E_p	ΔE^c	$\partial E_p/\partial \log v$	n^d	E_p	ΔE^c	$\partial E_p/\partial \log v$	n^d
c,*s*-DMU◇DMU	−2.34	45	−42	1.85	1.68	80	52	2.25
c,*s*-DMT◇DMT	−2.45	80	−62	1.75	1.67	80	52	1.95
t,*s*-DMU◇DMU	−2.34	42	−34	1.50	1.70	80	60	2.10
c,*a*-DMU◇DMU	−2.58	80	−50	1.85	2.05	60	42	3.50
c,*a*-DMT◇DMT	−2.61	80	−50	2.00	1.99	75	54	4.50
c,*a*-DMU^{6Me}◇DMU^{6Me}	−2.52	51	−39	1.95	2.02	65	45	3.75

[a] In DMF. [b] In ACN. [c] Peak width ($|E_{p/2} - E_p|$) at 0.1 V s^{-1}. [d] Electron stoichiometry.

c,*a*-DMU^{6Me}◇DMU^{6Me}, the peak widths at low scan rates indicate that the kinetics is already controlled by the charge transfer for *c*,*s*-DMU◇DMU but is still jointly determined by charge transfer and bond breaking for *c*,*a*-DMU^{6Me}◇DMU^{6Me}, meaning the chemical reaction is faster for the splitting of *c*,*s*-DMU◇DMU$^{\bullet+}$.

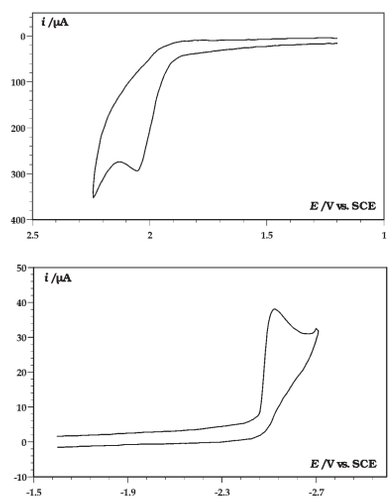

Fig. 6 Cyclic voltammetry of *c*,*a*-DMU^{6Me}◇DMU^{6Me}. Top: C = 1.50 mM, ACN + 0.1 M n-Bu_4NBF_4. Scan rate: 0.5 V s^{-1}. Temperature: 22 °C. Bottom: C = 1.01 mM in DMF + 0.1 M n-Bu_4NBF_4. Scan rate: 0.1 V s^{-1}. Temperature: 22 °C.

The reduction of *c*,*a*-DMU^{6Me}◇DMU^{6Me} involves a single irreversible wave, observed at −2.52 V *vs* SCE (0.1 V s^{-1}). The wave is thin (the peak-width amounts to 55 mV at low scan rates) while E_p shifts towards negative potentials at a rate of 39 mV per decade. This is again typical for a two-step process, with a mixed kinetic control between electron transfer and chemical reaction. That the peak potential smoothly changes to positive values while increasing the substrate concentration indicates the interference of a second order reaction. With an electron stoichiometry of n = 1.95, it can be assumed that the reduction mechanism of *c*,*a*-DMU^{6Me}◇DMU^{6Me} is similar to that of *c*,*s*-DMU◇DMU. It is difficult to compare the cleavage rate of *c*,*s*-DMU◇DMU$^{\bullet-}$ and *c*,*a*-DMU^{6Me}◇DMU$^{6Me\bullet-}$ since both peak width and $\partial E_p/\partial \log v$ are quite similar. It can nevertheless be concluded that *c*,*a*-DMU^{6Me}◇DMU^{6Me} is more difficult to reduce than *c*,*s*-DMU◇DMU on thermodynamic grounds, since the reduction wave of this latter compound is 180 mV more positive than that of *c*,*a*-DMU^{6Me}◇DMU^{6Me}. A voltammetric response is shown in Fig. 6.

The characteristics of both oxidative and reductive cleavages for all six dimers are compiled in Table 1. Comparison of the results obtained for *t*,*s*-DMU◇DMU and *c*,*s*-DMU◇DMU clearly shows that a *cis* or *trans* stereochemistry at the cyclobutane ring of the dimer has only marginal effects on both thermodynamics and kinetics of reduction and oxidation processes, since both wave shape (location, width, changes with the scan rate) and stoichiometry (n = 2) are very similar.

Comparison of the cleavage process of *c*,*s*-DMT◇DMT and *c*,*s*-DMU◇DMU (Table 1) reveals that changing from a uracil to thymine does not have a profund impact on the mechanism. An oxidation wave obtained at low scan rate is shown in Fig. 7. The first peak leads to the breaking of the dimer through a sequential pathway and involves the exchange of two electrons (n = 1.95), whereas the second peak corresponds to the oxidation of DMT produced during the cleavage process. Reduction of *c*,*s*-DMT◇DMT occurs at a potential slightly more negative than that of *c*,*s*-DMU◇DMU, E_p = −2.45 V *vs.* SCE, and the wave is also slightly larger ($E_{p/2} - E_p$ = 80 mV at 0.1 V s^{-1}). This likely reflects the more negative value of $E^0_{dimer/dimer^{\bullet-}}$ for *c*,*s*-DMT◇DMT.

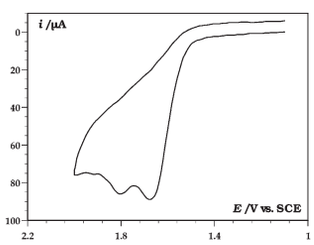

Fig. 7 Cyclic voltammetry of *c*,*s*-DMT◇DMT (2 mM) in ACN + 0.1 M n-Bu_4NBF_4. Scan rate: 0.1 V s^{-1}. Temperature: 22 °C.

Discussion and calculations

Thermodynamical parameters from reduction and oxidation of the dimers

Due to the slow electron transfer and the fast following chemical reaction, it was not possible to obtain standard potentials and cleavage rate constants for the dimer cleavage for both reduction and oxidation processes, neither from direct methods (high scan rate voltammetry) nor from indirect methods, such as redox catalysis. However, using the same strategy as applied for *c*,*s*-DMU◇DMU, one may take advantage of the finding that for several compounds, an increase of the scan rate quickly leads to kinetic control by charge transfer only. In these cases, the peak potential for an oxidative wave could be related to the standard potential and to the standard heterogeneous rate constant according to eqn. (3) and for a reductive wave according to eqn. (4).[9]

$$E_p = E^0_{dimer/dimer^{\bullet-}} - 0.78\frac{RT}{\alpha F} + \frac{RT}{\alpha F}\ln\left\{k_s^{app}\left(\frac{RT}{\alpha F v D}\right)^{1/2}\right\} \quad (4)$$

$E^0_{dimer/dimer^{\bullet-}}$ is the standard potential for dimer reduction and α is the transfer coefficient (close to 0.5). k_s^{app} was estimated by comparison with molecules of similar size to be 0.15–0.3 cm s^{-1}, The value for the diffusion coefficient D was estimated using the Stokes–Einstein equation to be on average 1.25 × 10^{-5} cm^2 s^{-1} in ACN and 6.6 × 10^{-6} cm^2 s^{-1} in DMF, since the hard sphere radii for all dimers under investigation are almost identical.[11]

With these data, the standard potential for dimer radical anion formation was calculated for *c*,*s*-DMT◇DMT, *c*,*a*-DMU◇DMU and *c*,*a*-DMT◇DMT, since in these cases complete kinetic control by charge transfer was achieved above 1 V s^{-1} (Table 2). Comparison of the standard potentials obtained for *c*,*s*-DMT◇DMT and *c*,*a*-DMT◇DMT indicates that a *syn* configuration stabilizes the radical anion by 150 mV over an *anti* configuration.

The standard potential for the formation of a dimer radical cation was calculated for *c*,*s*-DMT◇DMT and *t*,*s*-DMU◇DMU, using

Table 2 Estimation of standard potentials for reduction and oxidation of N,N-dimethyl thymine and uracil dimers, and for DMU and DMT monomers

Compound	$E°_{dimer/dimer^{\bullet-}}$ [a]	$E°_{dimer^{\bullet+}/dimer}$ [a]	$E°_{mono/mono^{\bullet-}}$ [ab]
c,*s*-DMU◇DMU	—	1.825 ± 0.025	≈ −2.39
c,*s*-DMT◇DMT	−2.620 ± 0.025	1.815 ± 0.025	≈ −2.46
t,*s*-DMU◇DMU	—	1.850 ± 0.025	
c,*a*-DMU◇DMU	−2.735 ± 0.025	≈2.195	
c,*a*-DMT◇DMT	−2.770 ± 0.025	—	

[a] In V *vs.* SCE. [b] Standard potential for the formation of monomer radical anion.[13]

eqn. (3) and taking into account that a slow limiting charge transfer is fully achieved around 1 V s^{-1} (Table 2). As already noticed, it appears that neither a *cis* or a *trans* configuration at the cyclobutane motif nor the presence or absence of a methyl group at the C(5)/C(5′) positions have a significant influence on the standard potential. The radical cations of *c*,*s*-DMU◇DMU, *c*,*s*-DMT◇DMT and *t*,*s*-DMU◇DMU should also cleave at comparable rates.

Interestingly, the *anti* dimer *c*,*a*-DMU◇DMU is the only compound (except *c*,*a*-DMU^{6Me}◇DMU^{6Me}), where, upon oxidation, the kinetics are jointly controlled by charge transfer and breaking of the C–C bond at low and moderate scan rates. In these cases, variation of peak width ΔE ($E_p - E_{p/2}$) and peak potential location E_p with log *v* depends on three parameters, *e.g.* $E°_{dimer^{\bullet+}/dimer}$, k_s^{app} and k_c, the cleavage rate of the C–C bond. Using an estimated value for k_s^{app} of 0.25 cm s^{-1} (mean value) and the experimentally determined values of ΔE and E_p, simulations of cyclovoltammetric curves were performed (Digisim, BioAnalytical System) to determine the standard potential and the cleavage rate constant. For *c*,*a*-DMU◇DMU we obtained $E°(dimer^{\bullet+}/dimer) \approx 2.195$ V *vs.* SCE and $k_c \approx 4 \times 10^6$ s^{-1}. Since the cleavage rate constant is quite sensitive to the exact value of k_s^{app}, k_c should be considered in terms of order of magnitude rather than an accurate absolute value. Nevertheless it can be concluded that *anti* dimers are substantially more difficult to oxidize than their *syn* homologues. As an example, in the case of *c*,*a*-DMU◇DMU the standard potential for radical cation formation is 370 mV more positive than that of *c*,*s*-DMU◇DMU (Table 2), indicating a destabilization of the radical cation state of *anti* dimers compare to *syn* compounds, as was already suggested by Pac *et al.*[14]

Modelling calculations

Mapping of the potential energy surface for a model compound[15] may give a more accurate view of the cleavage process in terms of electron reorganization, and may thus lead to a fundamental understanding of the origin of the activation barrier which is endowed, as shown experimentally, for both reductive and oxidative cleavage processes. To keep the required computation times at a reasonable level, density functional calculations (using the B3LYP/6–31G* method) were performed for simplified cyclobutane adduct models in order to get a refined qualitative description of the pyrimidine reformation, rather than a quantitative estimation of the size of the cleavage barriers.

The minimum energy pathway for the homolytic cleavage of $\mathbf{A}^{\bullet-}$(Fig. 8) was calculated in mass-weighted internal coordinates (IRC), revealing that the C(5)–C(5′) bond cleaves first with a free enthalpy of activation of $\Delta G^{\ddagger} = 0.21$ eV (Fig. 9) (it was verified that C(6)–C(6′) bond breaking is far less favorable). It should be noted that the activation barrier in solution is certainly slightly higher, since a small percentage (10%) of the negative charge located onto the C(4)=O(4) group is transfered to the C(5′) atom when reaching the transition state, thus leading to an additional solvent reorganization energy. At the transition state (**TS1**, Fig. 9), C(5)–C(5′) elongates from 1.569 to 1.937 Å, and almost 40% of spin density locates onto the C(5′) atom [in the ground state geometry of $\mathbf{A}^{\bullet-}$ only 5% of the spin is located on C(5′)]. This indicates that an intramolecular electron transfer occurs during this first homolytic cleavage. The pathway then leads to a second minimum (**2**, Fig. 9), before reaching a second barrier (**TS2**, Fig. 9), which corresponds to the breaking of the C(6)–C(6′) bond, a step endowed with a smaller barrier of $\Delta G^{\ddagger} = 0.11$ eV. From structure **2** to **TS2**, the C(6)–C(6′) bond length increases from 1.585 to 2.049 Å. At the same time, the spin on C(5′), which is close to 1 in state **2**, decreases to 0.58 in **TS2** and finally drops to zero as the enamine leaving group is formed (CH_2CHNH_2). At the end of the cleavage process, the spin is mainly localized on C(6), which corresponds to the radical anion state of uracil. The spin density repartition on the various atoms all along the reactive pathway is summarized in Table 3.

Table 3 Gas phase reduction of a model compound of cyclobutane pyrimidine dimer (A + $1e^-$). Spin repartition along the reaction pathway

	C(4)	O(4)	C(5)	C(5)′	C(6)
1	0.52	0.26	0	0.05	0.01
TS1	0.29	0.22	0.04	0.38_5	0.02
2	0	0.02	0.06	0.97	0.01
TS2	0.03	0.06	0.14	0.58	0.19
3	0.13	0.12	0.09	0	0.57

These calculations confirm our suggestion made for the reductive cleavage of *c*,*s*-DMU◇DMU that the C(5)–C(5′) bond breaks first

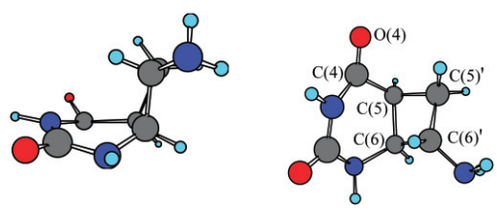

Fig. 8 Model compound ($\mathbf{A}^{\bullet-}$) sketching cyclobutane pyrimidine dimer reduction. Optimized radical anion geometry (right: top view).

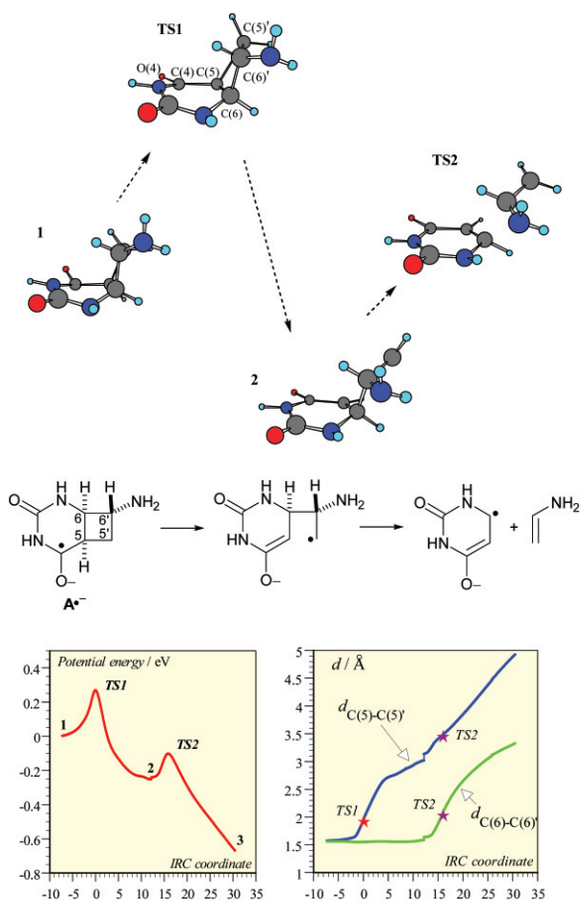

Fig. 9 Gas phase reduction of pyrimidine dimer adduct model **A**. Top: structures at minima (**1**, **2**) and at transition states (**TS1**, **TS2**). Bottom: Potential energy at the B3LYP/6–31G* level (left) and C–C bond distances (right) as a function of the mass-weighted IRC coordinate (reaction coordinate in $u^{-1/2}$ a_0).

with a sizable activation barrier. In a second step, the C(6)–C(6′) elongates to lead to the formation of the two monomeric DMU.

It was not possible to locate transition states for the homolytic cleavage of of the cyclobutane ring in $\mathbf{A}^{\bullet+}$. However, calculations performed for model compound $\mathbf{B}^{\bullet+}$ (Fig. 10) revealed that the oxidative cleavage goes through an activation barrier, corresponding to the splitting of the C(6)–C(6′) bond firstly. The free enthalpy of activation is calculated to be $\Delta G^{\ddagger} = 0.03$ eV, whereas the alternative cleavage of the C(5)–C(5′) bond is much less favorable. From the optimized radical cation geometry to the transition state, C(6)–C(6′) elongates from 1.791 to 1.95 Å, while the spin density on C(6′) increases from 35% to 50%. At the same time, the spin density on N(1) decreases from 42% to 31%, thus indicating an intramolecular electron transfer to the $\sigma^*_{C(6)-C(6)'}$ orbital. In a subsequent step the C(5)–C(5′) bond breaks, but it was not possible to characterize a transition state for this second cleavage.

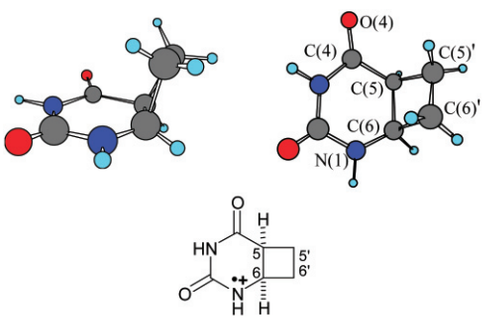

Fig. 10 Model compound ($\mathbf{B}^{\bullet+}$) used for simulating cyclobutane pyrimidine dimer oxidation. Optimized radical cation geometry (upper right: top view).

Consequences for the enzymatic repair mechanism

It is remarkable that monomers and dimers have comparable standard redox potentials (see Table 2, reduction reaction), stressing the importance of the structure of the damaged DNA/photolyase complex and the position of dimer motif inside the catalytic site, which should be brought close to the cofactor.[2c,16]

We have shown that the reductive cleavage of model dimers follows a two steps sequential pathway at an electrode. Since driving forces in photoinduced electron transfer reactions are higher, it is tempting to conclude that the enzymatic repair by photolyase enzymes should also proceed through intermediate formation of a dimer radical anion. Indeed, the reducing power of the excited flavin cofactor $^1FADH^-$* amounts to −3.24 V *vs* SCE, since the first excited state energy is 2.76 eV[2c] and the standard redox potential for $FADH^-$ oxidation equals −0.48 V *vs.* SCE, as was estimated from the reversible voltamograms obtained in aqueous buffered solutions of riboflavin (Fig. 11).

However, in a recent thymidine repair study by DNA photolyase in real time (picosecond range), the data shown by Stanley *et al.* strongly suggest that the first carbon–carbon bond cleavage and electron transfer are concerted processes.[17] Crystal structures have shown

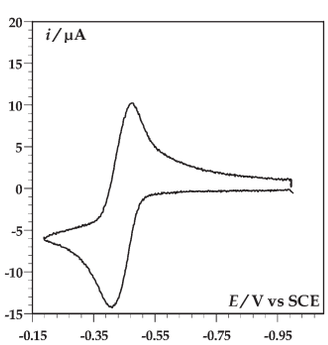

Fig. 11 Cyclic voltammetry of riboflavin (1.48 mM) + dithionite (1 eq.) in aqueous buffered solution (Buffer Tris, $C = 0.05$ M, pH = 7.3). Scan rate: 0.1 V s^{-1}. Temperature: 22 °C.

that the canonical DNA structure is lost locally at the catalytic site,[18] so that the dimer is certainly under considerable strain upon binding to photolyase. It is therefore possible that the $\sigma^*_{C(5)-C(5)'}$ orbital is sufficiently stabilized (through elongation) to render the concerted path more favorable than the stepwise. Thus, the concerted or sequential nature of the first electron transfer/bond breaking reaction of the reductive repair sequence could not be infered only from model studies. Nevertheless, a qualitative description of the repair reaction in terms of reaction pathway is possible, as is illustrated in Fig. 12 for the reduction of a thymine dimer (T◇T) by excited $FADH^-$.

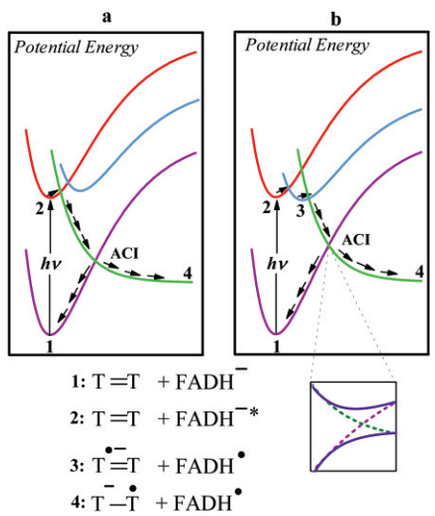

Fig. 12 Diabatic potential energy profiles (zero order) for the redox reaction between the flavin cofactor ($FADH^-$) and a thymine dimer (T=T). a: Concerted pathway. b: Sequential pathway going through the radical anion state $T{=}T^{\bullet-}$. The inset on diagram b details the avoided crossing intersection (ACI zone) between the ground state reactants and products energy curves (dotted lines: zero order profile, full lines: first order profile).

A sequential pathway is outlined in diagram (b). After photon absorption (formation of **2**) and electron transfer to the dimer *via* a small activation barrier (**2** → **3**), the short lived radical anion (**3**) then breaks through a second activation barrier, to give the fragmented dimer **4**. The restored bases resulting from fragmention of **4** (cleavage of a second C–C bond) and subsequent rapid oxidation are not sketched in the diagram (this process is highly exergonic and goes through a small, if any, activation barrier). Before reaching **4**, the system crosses the intersection between the potential energy surface of the fragmented state and that of the initial ground state (ACI). There, it partitions between the two surfaces thus concurrently heading for the fragments and for the initial ground state.[19] The degree of partitioning is a function of the degree of mixing of the two states, *i.e.* of the degree of avoided crossing, at the intersection.

This avoided crossing return electron transfer is responsible for a lowering of the quantum yield, which may asymptotically reach a value of 0.5 upon increasing the avoided crossing energy.[19a,b] This should be the main reason why the quantum yield for repair is less than one. The non concerted character of the process should have no influence on the repair yield because back electron transfer at the level of the radical anion (**3** → **1**) is lying deep in the Marcus inverted region and is thus not competitive with the rapid C(6)–C(6′) fragmentation. In fact, the driving force for the charge transfer reaction **2** → **3** is −0.62 eV, as indicated from our experimentally determined standard potential values for the two redox couples $FADH^{\bullet}/FADH^-$ and *c*,*s*-DMT◇DMT/*c*,*s*-DMT◇$DMT^{\bullet-}$. The back electron transfer **3** → **1** is thus exergonic with a driving force of about −2.14 eV (−2.76 + 0.62), to be compared to a reorganization energy around a likely value of 1 eV.

The second possible pathway, a concerted electron transfer/bond breaking reaction (**2** → **4**), is depicted on the left part of Fig. 12 (diagram a). This is a highly exergonic process, which is endowed with a large intrinsic barrier, due to the contribution of the bond being broken during the process. The strain at the dimer motif bound to the enzyme may lower the barrier for this pathway, leading to a kinetic

advantage over the sequential pathway. In this case, the system, *en route* to **4**, again crosses the intersection between the potential energy surface of the fragmented state and that of the initial ground state (ACI). This means that the quantum yield for the repair would also be controlled by the partitioning at the intersection.[19a]

It is therefore not surprising that the quantum yields (Φ) for repair by the enzyme containing $FADH^-$ are 0.7–1.[2c] Whatever may be the pathway followed (concerted or sequential), and even if this pathway may be different from one dimer stereochemistry to an other, Φ mainly depends from the crossing of the ground state reactant and products curves (ACI region, Fig. 12). The high values of Φ reflect the fact that the crossing is moderately adiabatic and weakly sensitive to the dimer structure and stereochemistry.

Conclusions

Pyrimidine cyclobutane dimers are cleaved under both reductive and oxidative conditions at a carbon electrode. *En route* to cleavage, ion radical intermediates are formed prior to two successive homolytic C–C bond cleavages, leading to the formation of the neutral monomeric base and the ion radical of the monobase. The former species undergoes further electron exchange, since it's formed at a potential beyond it's standard redox potential. *Syn* dimers are more easily oxidized and reduced than *anti* structures, while only marginal changes are observed upon alkyl substitution at the cyclobutane motif. The cleavage rate constants of the dimers were too fast to be measured, but a careful analysis of the shape of the voltammetric curves allows the estimation of the standard potential for the formation of the radical anion for *c*,*s*-DMT<>DMT, *c*,*a*-DMU<>DMU, *c*,*a*-DMT<>DMT, while the standard potential for the formation of the radical cation for *c*,*s*-DMU<>DMU, *c*,*s*-DMT<>DMT, *t*,*s*-DMU<>DMU and *c*,*a*-DMU<>DMU were obtained. Radical anions of *syn* dimers are stabilized over those of *anti* configuration by *ca.* 150 mV while radical cation of *syn* compounds are stabilized over those of *anti* configuration by *ca.* 350 mV. The barrier for cleavage of the intermediate mainly originates in an intramolecular electron transfer from the orbital where the unpaired electron temporarily sites to the σ* of the carbon–carbon bond being broken, a contribution to which solvent reorganization energy should be added. The standard potential for the formation of the radical anion of the monobases (DMU and DMT) are more positive than those of all the dimers investigated. In the catalytic site where photolyase enzyme repair such dimer adducts on DNA strands, the lesion is flipped out the double strand, and is thus brought in close contact to the cofactor. The strain at the dimer motif probably facilitates the reductive cleavage and may even render the fully concerted pathway more favorable than the stepwise mechanism observed under our electrochemical conditions for model compounds. But whatever may be the pathway followed inside the enzyme, the repair quantum yield is likely to be controlled by the crossing of the two surfaces associated to fragmented dimer and the reactants respectively, which should be moderately adiabatic, in accordance with the high efficiency of the enzymatic repair.

Experimental

Chemicals

N,*N*′-dimethyl formamide (Fluka, > 99.8%, stored over molecular sieves and under argon atmosphere), acetonitrile (Fluka, > 99.5%, stored over molecular sieves and under argon atmosphere), acetone (Acros, HPLC grade, 99.8%), the supporting electrolyte *n*-Bu_4NBF_4 (Fluka, > 99%), uracil (Sigma), thymine (Sigma), 1,3-dimethyluracil (Aldrich), riboflavin (Sigma) and sodium dithionite (Aldrich) were used as received.

Synthesis of the pyrimidine cyclobutane dimers

1,3-Dimethylthymine (DMT) was synthesized following the procedure described by Falvey and coworkers.[20]

1,3,6-Trimethyluracil (DMU^{6Me}) was prepared according to reference 21a.

DMU<>DMU. In a pyrex reactor 520 mg (3.71 mmol) DMU was dissolved in 100 mL of acetone and deaerated in an ultrasonic bath by bubbling argon through the solution. The reaction mixture was irradiated under argon for 10 h using a medium-pressure mercury lamp. After evaporation of the solvent *in vacuo* the residue was purified by chromatography to yield the various DMU<>DMU isomers in 75% combined yield. The stereoconfiguration of the isomers was assigned by comparison with literature data.[21b]

DMT<>DMT. In a pyrex reactor 680 mg (4.42 mmol) DMT was dissolved in 100 mL of acetone and deaerated in an ultrasonic bath by bubbling argon through the solution. The reaction mixture was irradiated under argon for 3 d using a medium-pressure mercury lamp. After evaporation of the solvent *in vacuo* the residue was purified by chromatography to yield the various DMT<>DMT isomers in 55% combined yield. The stereoconfiguration of the isomers was assigned by comparison with literature data.[21c]

DMU^{6Me}<>DMU^{6Me}. In a pyrex reactor 1.01 g (6.56 mmol) DMU^{6Me} was dissolved in 100 mL of acetone and deaerated in an ultrasonic bath by bubbling argon through the solution. The reaction mixture was irradiated under argon for 4 d using a medium-pressure mercury lamp. After evaporation of the solvent *in vacuo* the residue was purified by chromatography to yield the various DMU^{6Me}<>DMU^{6Me} isomers in 95% combined yield. The stereoconfiguration of *c*,*a*-DMU^{6Me}<>DMU^{6Me} was assigned by X-ray analysis.[21d] Yield: 69%; $R_f = 0.19$ (SiO_2, ethyl acetate); mp. 206–207 °C (colourless solid); ν_{max} (KBr)/cm^{-1}: 2980, 1698, 1664, 1458, 1342; δ_H ($CDCl_3$, 300 MHz): 3.22 [6H, s, N(3)CH_3, N(3′)CH_3], 3.18 (2H, s, 5-H, 5′-H), 2.83 [6H, s, N(1)CH_3, N(1′)CH_3], 1.66 (6H, s, 6-CH_3, 6′-CH_3); δ_C ($CDCl_3$, 75.5 MHz): 165.1 (s, C-4, C-4′), 151.9 (s, C-2, C-2′), 57.9 (s, C-6, C-6′), 53.4 (d, C-5, C-5′), 31.0 [q, N(1)CH_3, N(1′)CH_3], 28.1 [q, N(3)CH_3, N(3′)CH_3], 27.7 (6-CH_3, 6′-CH_3); *m*/*z* (EI): 154 (100), 97 (49), 82 (25); *m*/*z* (CI): 155 (100); $C_{14}H_{20}N_4O_4 \cdot 0.1\ C_4H_8O_2$: calcd. C 54.33, H 6.59, N 17.60; found C 54.39, H 6.61, N 17.72.

Electrochemical experiments

All substrates were studied by cyclic voltammetry in *N*,*N*′-dimethyl formamide (DMF, reduction) or acetonitrile (ACN, oxidation). The working electrode was a 3 mm-diameter glassy carbon electrode disk (Tokai) carefully polished and ultrasonically rinsed in absolute ethanol before use. The counter-electrode was a platinum wire and the reference electrode an aqueous SCE electrode. The potentiostat, equipped with a positive feedback compensation and current measurer was the same as previously described.[22] All experiments have been done at 22 °C, the double-wall jacket cell being thermostated by circulation of water.

Molecular modelling

All the calculations were performed with the Gaussian 98 series of programs.[23] DFT (B3LYP) method and 6-31G* basis set were used. Minimum energy structures were fully optimized. Frequency calculations were made to verify that the structures were minima (no imaginary frequencies) or saddle point (one imaginary frequency) and to evaluate thermodynamical functions.

The nature of the reactant and products linked to transition states was assigned by the intrinsic reaction coordinate (IRC) method at the same level of calculation as used for saddle point characterization. IRC's have been determined in mass-weighted internal coordinates with a step size of 0.05 or 0.1 in atomic units. The activation barriers were calculated as the free enthalpy difference between the saddle point and the minimum structures.

Notes and references

1 T. Douki, A. Reynaud-Angelin, J. Cadet and E. Sage, *Biochemistry*, 2003, **42**, 9221–9226.
2 (*a*) P. F. Heelis, R. F. Hartman and S. D. Rose, *Chem. Soc. Rev.*, 1995, 289–297; (*b*) T. Carell, L. T. Burgdorf, L. M. Kundu and M. Cichon,

Curr. Opin. Chem. Biol., 2001, **5**, 491–498; (*c*) A. Sancar, *Chem. Rev.*, 2003, **103**, 2203–2237, and references cited theirein.

3 (*a*) G. Prakash and D. E. Falvey, *J. Am. Chem. Soc.*, 1995, **117**, 11375–11376; (*b*) X. Zhao, J. Liu, D. S. Hsu, S. Zhao, J. S. Taylor and A. Sancar, *J. Biol. Chem.*, 1997, **272**, 32580–32590; (*c*) J. Arul, G. Prakash and D. E. Falvey, *J. Am. Chem. Soc.*, 2000, **122**, 11219–11225; (*d*) K. Hitomi, H. Nakamura, S. T. Kim, T. Mizukoshi, T. Ishikawa, S. Iwai and T. Todo, *J. Biol. Chem.*, 2001, **276**, 10103–10109.

4 (*a*) J.-M. Savéant, in *Advances in Physical Organic Chemistry*, ed. T. T. Tidwell, Academic Press, New York, 2000, vol. 35, 117–192; (*b*) L. Pause, M. Robert and J.-M. Savéant, *J. Am. Chem. Soc.*, 2001, **123**, 4886–4895; (*c*) C. Costentin, M. Robert and J. M. Savéant, *J. Am. Chem. Soc.*, 2003, **125**, 105–112.

5 (*a*) U. Wille, in *Highlights in Bioorganic Chemistry: Methods and Applications* ed. C. Schmuck and H. Wennemers, Wiley-VCH, Weinheim, 2004, 352–368; (*b*) O. Krüger and U. Wille, *Org. Lett.*, 2001, **3**, 1455–1458; (*c*) R. J. Robbins and D. E. Falvey, *J. Org. Chem.*, 1993, **58**, 3616–3618; (*d*) K. Okada, K. Hisamitsu and T. Mukai, *J. Chem. Soc., Chem. Commun.*, 1980, 941–942; (*e*) K. Okada, K. Hisamitsu, T. Miyashi and T. Mukai, *J. Chem. Soc., Chem. Commun.*, 1982, 974–976; (*f*) C. Pac, *Pure Appl. Chem.*, 1986, **58**, 1249–1256.

6 See for example: (*a*) E. M. Boon, N. M. Jackson, M. D. Wightman, S. O. Kelley, M. G. Hill and J. K. Barton, *J. Phys. Chem. B.*, 2003, **107**, 11805–11812; (*b*) T. Ito and S. E. Rokita, *J. Am. Chem. Soc.*, 2003, **125**, 11480–11481; (*c*) T. Carell, C. Behrens and J. Gierlich, *Org. Biomol. Chem.*, 2003, **1**, 2221–2228.

7 (*a*) C. Behrens, M. Obber and T. Carell, *Eur. J. Org. Chem.*, 2002, 3281–3289; (*b*) C. Behrens and T. Carell, *Chem. Commun.*, 2003, 1632–1633; (*c*) S. Breeger, U. Hennecke and T. Carell, *J. Am. Chem. Soc.*, 2004, **126**, 1302–1303.

8 (*a*) T. E. Cummings and P. J. Elving, *J. Electroanal. Chem.*, 1978, **94**, 123–145; (*b*) T. E. Cummings and P. J. Elving, *J. Electroanal. Chem.*, 1979, **102**, 237–248; (*c*) Y. Huang and H. Kenttämaa, *J. Phys. Chem. A*, 2003, **107**, 4893–4897.

9 L. Nadjo and J.-M. Savéant, *J. Electroanal. Chem.*, 1973, **48**, 113–145.

10 It is known that vinylarylsulfones and vinyl pyridines undergo cyclodimerization at the level of the radical anion within catalytic amounts of charge (see for example J. F. Bergamini, J. Delaunay, P. Hapiot, M. Hillebrand, C. Lagrost, J. Simonet and E. Volanschi, *J. Electroanal. Chem.*, 2004, **569**, 175–184; R. G. Janssen, M. Motevalli and J. H. P. Utley, *Chem. Commun.*, 1998, 539–540). This process involves a neutral molecule and its radical anion and is accompanied with a significant activation barrier. Our observation that the electron stoichiometry for pyrimidine monomer reduction remains unchanged even at very low scan rates and the excellent reproducibility of the reduction wave during the cycling experiments indicate that a cyclodimerization process as described for vinylarylsulfones and vinyl pyridines did not occur in our case. In contrast, dimerization of the pyrimidine monomer radical anions at the C(6) position only involves minor electronic reorganization and is likely endowed with only a negligible if any activation barrier, thus making this step nearly diffusion controlled.

11 The diffusion coefficient D was estimated through application of the Stokes–Einstein equation $D = k_B T/(6\pi\eta a)$, η being the solvent viscosity and a the hard sphere radius equivalent to the diffusing molecule. Radii were obtained from a quantum calculation at the B3LYP level (keyword Volume). Typically, values close to 4.7 Å were found and vary only marginally from one dimer to an other. Thus D was taken equal to 1.25 10^{-5} cm^2 s^{-1} in ACN and to 6.6 10^{-6} cm^2 s^{-1} in DMF for all compounds.

12 S. T. Kim and A. Sancar, *Biochemistry*, 1991, **30**, 8623–8630.

13 Simulation of the experimental curves with Digisim (BioAnalytical System) leads to the reported values. Three parameters control the shape and the position of the wave: the standard potential, the rate constant for radical anion dimerization and the heterogenous electron transfer rate constant, k_s^{app}. The two last parameters were estimated to 10^9 M^{-1} s^{-1} and 0.1 cm s^{-1} respectively, leading to the sole variation of the standard potential for adjustment with the experimental voltammetric curves. The uncertainty on the $E°$'s obtained is estimated to equal 25 mV.

14 C. Pac, J. Kubo, T. Majima and H. Sakurai, *Photochem. Photobiol.*, 1982, **36**, 273–282.

15 (*a*) A. Voityuk, M.-A. Michel-Beyerle and N. Rösch, *J. Am. Chem. Soc.*, 1996, **118**, 9750–9758; (*b*) A. Voityuk and N. Rösch, *J. Phys. Chem. A*, 1997, **101**, 8335–8338; (*c*) M. Aida, F. Inoue, M. Kaneko and M. Dupuis, *J. Am. Chem. Soc.*, 1997, **119**, 12274–12279; (*d*) J. Rak, A. Voityuk and N. Rösch, *J. Phys. Chem. A*, 1998, **102**, 7168–7175; (*e*) B. Durbeej and L. A. Eriksson, *J. Am. Chem. Soc.*, 2000, **122**, 10126–10132.

16 J. Antony, D. M. Medvedev and A. A. Stuchebrukhov, *J. Am. Chem. Soc.*, 2000, **122**, 1057–1065.

17 A. W. MacFarlane IV and R. J. Stanley, *Biochemistry*, 2003, **42**, 8558–8568.

18 (*a*) H. Komori, R. Masui, S. Kuramitsu, S. Yokoyama, T. Shibata, Y. Inoue and K. Miki, *Proc. Natl. Acad. Sci., USA*, 2001, **98**, 13560–13565; (*b*) K. S. Christine, A. W. MacFarlane IV, K. Yang and R. J. Stanley, *J. Biol. Chem.*, 2002, **41**, 38339–38344; (*c*) H. Park, K. Zhang, Y. Ren, S. Nadji, N. Sinha and J.-S. Taylor, *Proc. Natl. Acad. Sci., U. S. A.*, 2002, **99**, 15965–15970.

19 (*a*) M. Robert and J.-M. Savéant, *J. Am. Chem. Soc.*, 2000, **122**, 514–517; (*b*) C. Costentin, M. Robert and J.-M. Savéant, *J. Phys. Chem. A*, 2000, **104**, 7492–7501.

20 M. P. Scannell, G. Prakash and D. E. Falvey, *J. Phys. Chem. A*, 1997, **101**, 4332–4337.

21 (*a*) H. Egg and I. Volgger, *Synthesis*, 1982, 1071–1073; (*b*) P. Maul, E. Fahr, K.-A. Lehner and D. Scheutzow, *Z. Naturforsch. B*, 1972, **27**, 1481–1484; (*c*) H. Morrison and R. Kloepfer, *J. Am. Chem. Soc.*, 1972, **94**, 255–264; (*d*) C. Näther, O. Krüger and U. Wille, *Acta Cryst.*, 2002, **E58**, 405–406.

22 D. Garreau and J.-M. Savéant, *J. Electroanal. Chem.*, 1972, **35**, 309–331.

23 M. J. Frisch, G. W. Trucks, H. B. Schlegel, M. A. Scuseria, P. M. W. Gill, B. G. Johnson, M. A. Robb, J. R. Cheeseman, T. Keith, G. A. Petersson, J. A. Montgomery, R. E. Stratmann, J. C. Burant, S. Dapprich, J. M. Millam, A. D. Daniels, K. N. Kudin, M. C. Strain, O. Farkas, J. Tomasi, V. Barone, M. Cossi, R. Cammi, B. Mennuci, C. Pomelli, C. Adamo, S. Clifford, G. Ochterski, Q. Cui, K. Morokuma, D. K. Malick, A. D. Rabuck, K. Raghavachari, M. A. Al-Laham, V. G. Zakrzewski, J. V. Ortiz, J. B. Foresman, J. Cioslowski, B. B. Stefanov, G. Liu, A. Liashenko, P. Piskorz, I. Komaromi, A. Nanayakkara, M. Challacombe, C. Y. Peng, P. Y. Ayala, W. Chen, M. W. Wong, J. L. Andres, A. S. Replogle, R. Gomperts, R. L. Martin, D. J. Fox, J. S. Binkley, D. J. Defrees, J. Baker, J. P. Stewart, M. Head-Gordon, C. Gonzalez, J. A. Pople, *Gaussian 98, Revision A.1*, Gaussian, Inc., Pittsburgh, PA, 1998.